

Low-Dimensional Models for Real Time Simulations of Catalytic Monoliths

Saurabh Y. Joshi, Michael P. Harold, and Vemuri Balakotaiah

Dept. of Chemical and Biomolecular Engineering, University of Houston, Houston, TX 77204-4004

DOI 10.1002/aic.11794

Published online May 27, 2009 in Wiley InterScience (www.interscience.wiley.com).

We present accurate low-dimensional models for real time simulation, control, and optimization of monolithic catalytic converters used in automobile exhaust treatment. These are derived directly by averaging the governing equations and using the concepts of internal and external mass transfer coefficients. They are expressed in terms of three concentration and two temperature modes and include washcoat diffusional effects without using the concept of the effectiveness factor. The models reduce to the classical two-phase models in the limit of vanishingly thin washcoat. The models are validated by simulating the transient behavior of a three-way converter for various cases and comparing the predictions with detailed solutions. It is shown that these new models are robust and accurate with practically acceptable error, speed up the computations by orders of magnitude, and can be used with confidence for the real time simulation and control of monolithic and other catalytic reactors. © 2009 American Institute of Chemical Engineers AIChE J, 55: 1771–1783, 2009

Keywords: catalytic monolith, averaging, convection-diffusion-reaction equation, washcoat diffusion, internal and external mass transfer coefficients

Introduction

The monolithic catalytic reactor is widely used in treating the exhaust from gasoline powered vehicles, catalytic oxidation of VOCs, removal of NO_x from lean burn and diesel engines, power plant, and furnace exhaust gases. It has several advantages such as high heat and mass transport rates per unit pressure drop, smaller transverse temperature gradients and ease of scale-up, when compared with the traditional packed-bed reactor. The monolith reactor consists of a large number of long, narrow channels (of hydraulic diameter about 1 mm) in parallel through which reacting fluid flows and the catalyst is deposited in the form of washcoat (of average thickness about 20 μ m) on the monolith channel wall. The reactants diffuse transverse to the flow direction in the gas phase and through the porous washcoat where they react and the products formed diffuse back into the gas phase. Therefore, detailed mathematical models of a mono-

lith reactor consist of a system of coupled nonlinear partial differential equations (PDEs) in at least two spatial dimensions (axial and radial/transverse) and time along with highly nonlinear reaction source/sink terms appearing in the solid phase species and energy balances. Although the numerical solution of such detailed models with complex catalytic chemistry is possible with the present day computers, it may be demanding in terms of time and memory requirements, especially for real time simulations that may be needed in the control and optimization schemes. In addition, detailed solutions, even when available, have to be coarse grained to obtain quantities of practical interest, such as the average exit conversion of a reactant. For strongly nonlinear reactor models exhibiting multiple solutions and boundary layers, determination of the different types of solutions that may exist in the multidimensional parameter space may be computationally prohibitive. For these reasons, it is desirable to have simplified low-dimensional models having same qualitative behavior as the full PDE models and sufficient accuracy for practical applications.

The most commonly used simplified models of catalytic monoliths are the 1-D two-phase models (Froment and

Correspondence concerning this article should be addressed to M. P. Harold mharold@uh.edu or V. Balakotaiah at bala@uh.edu

Bischoff¹; Oh and Cavendish²; Hayes et al.³). These models use two modes (or two different concentrations/temperatures) and the concept of effective external heat and mass transfer coefficients between the solid and fluid to account for the transverse variations caused due to velocity gradients and diffusion of reactant species or heat in the fluid phase. Many experimental (Hawthorn⁴; Ullah and Waldram⁵; Uberoi and Pereira⁶; Holmgren and Andersson⁷; and West et al.⁸) as well as theoretical (Shah and London⁹; Groppi and Tronconi¹⁰; Tronconi and Forzatti¹¹; Hayes and Kolaczowski¹²; Gupta and Balakotaiah¹³; and Balakotaiah and West¹⁴) correlations have been developed and validated in the literature for these effective external transfer coefficients. A major limitation of most of these classical two-phase models is that they neglect the temperature or concentration gradients within the washcoat or assume chemical reactions occur only on the surface of the catalytic wall. This assumption restricts the application of these models to low temperatures or low catalyst activity and/or loading, or to the case of extremely thin washcoats. The concentration gradients within the washcoat may become significant at higher temperatures or when the diffusion in the washcoat is in the Knudsen regime. To account for the washcoat diffusional effect, the classical two-phase models can be extended using the concept of effectiveness factor to simplify the problem of diffusion and reaction in the washcoat.¹ However, this approach increases the computational effort tremendously as it requires the solution of the multicomponent diffusion and reaction problem in the transverse coordinates (at each axial location) to determine the interphase fluxes. In addition, this approach as used in the literature has its limitations (and conceptual difficulties), especially for the case of multiple reactions, time varying inlet and transient conditions and has not been validated, for example, by comparing the two-phase model solution with that of the full governing equations. The recent experimental work of Santos and Costa^{15,16} underscores the importance of including washcoat diffusional effects in the transient modeling of three-way catalytic converters (TWCs).

At the next level, the models of monoliths include detailed kinetics or catalytic reaction mechanisms (instead of overall reactions and global kinetic expressions) along with washcoat diffusional limitations. Mukadi and Hayes¹⁷ modeled TWC with mechanistic kinetics using the Newton-Krylov method and showed that washcoat diffusion limitations are very significant even at relatively low operating temperatures. Koci et al.¹⁸ simulated monolithic converters with microkinetics and considered washcoat diffusional limitations using the short monolith and the plug flow models. Although these studies capture more details from the macro down to the microscale, they are prohibitive in terms of numerical effort, and impractical for the purpose of real time simulation, reactor control, and optimization. Further, they assume that the microkinetic mechanisms and rate constants are known, while in most practical situations, which they estimated using macroscale experimental data (Koltsakis et al.¹⁹). This kinetic parameter estimation is a nontrivial task if the full PDE models are used.

The next detailed level models of monoliths assume that the flow conditions in the different channels of the monolith are identical and solve the full 3-D governing (momentum,

species, and energy balance) equations for a single representative channel.^{20–22} Finally, the most detailed models of monolithic reactors consider the flow and temperature variations across the channels and the thermal coupling between the channels.²³

Prior work on the modeling of catalytic reactors has shown that the simplified models such as the classical two-phase models that include washcoat diffusional effects can describe the qualitative behavior of monolithic reactors and also have the quantitative accuracy needed for most practical applications. The derivation and validation of such low-dimensional models is the focus of the current work.

In this work, we derive multimode low-dimensional models for washcoated monoliths that are generalizations of the classical two-phase models. Specifically, we reduce the transverse degrees of freedom by averaging the convection-diffusion-reaction (CDR) equations in the transverse direction and using the concept of internal and external mass transfer coefficients. In the next section, we consider the case of an isothermal monolith reactor and present a three-mode low-dimensional model. We validate it by comparing its solution to the exact solution of the CDR equations. We then extend the low-dimensional model for nonisothermal and transient analysis of a catalytic monolith in which CO oxidation occurs. Finally, we present the extension of a five mode low-dimensional model to the most general case of multiple reactions under nonisothermal conditions and the application of this model for real time simulation of three-way converters (TWCs) and other monolithic reactors.

Formulation of Detailed Model

In this section, we present a detailed mathematical model of a catalytic monolith. We consider a single straight channel of arbitrary shape in which the catalyst is distributed uniformly within the porous washcoat deposited on the inner wall of the channel. It is assumed that the cross-section of the channel is invariant with the axial position, but the washcoat thickness may vary along the circumferential perimeter, as shown in Figure 1. This represents more realistic shape of monoliths used in practical applications, for example, monoliths in which washcoat is deposited on the interior of a square, rectangular, or triangular channel where it tends to deposit more at the corners, making washcoat thickness non-uniform along the periphery. Further, we make the following assumptions while developing the detailed convection-diffusion-reaction model: (i) the flow is laminar and fully developed; (ii) the aspect ratio of the channel is assumed to be small, that is, the hydraulic diameter of the channel is much smaller than the length of the channel. Assumption (ii) justifies the use of fully developed velocity profile neglecting entry region effects or developing flow conditions and also leads to the simplification of negligible axial diffusion in both the fluid phase and washcoat when compared with the convective transport; (iii) isothermal conditions; (iv) variations of physical properties with composition are neglected; and (v) the rate of disappearance of the limiting reactant per unit volume of the washcoat may be expressed in terms of the gas-phase mole fraction or concentration of the reactant in the washcoat. Most of these assumptions will be relaxed later when the model equations are extended to the general

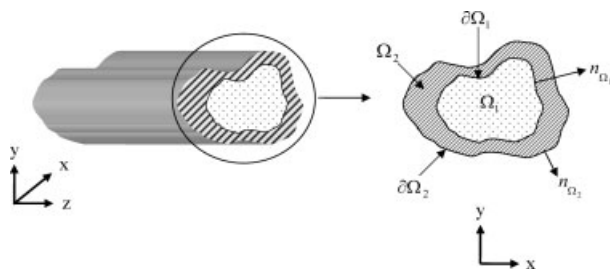


Figure 1. Schematic diagram illustrating the notations and different domains in a monolithic channel of arbitrary shape.

case. With these assumptions, the detailed convection-diffusion-reaction model in dimensional form is given by

$$\frac{\partial C_1}{\partial t} + \langle u \rangle f(x, y) \frac{\partial C_1}{\partial z} = D_f (\nabla_T^2 C_1) \quad 0 < z < L, (x, y) \in \Omega_1 \quad (1)$$

$$\varepsilon_{wc} \frac{\partial C_2}{\partial t} = D_s (\nabla_T^2 C_2) - R(C_2) \quad 0 < z < L, (x, y) \in \Omega_2 \quad (2)$$

Here, C_1 and C_2 are the reactant concentration in the fluid and catalyst (washcoat), respectively. Ω_1 and Ω_2 denote the cross-sectional domains of the fluid phase and catalyst (washcoat), respectively; L is the length of the channel; ∇_T^2 is the transverse Laplacian operator in Ω_1 and Ω_2 , D_f is the molecular diffusivity of the reacting species in the fluid phase, D_s is effective diffusivity of the reacting species within the washcoat, $\langle u \rangle$ is the average velocity, and $f(x, y)$ is the (normalized) local velocity profile within the channel (other symbols are defined in the notation). Equation 2 is subjected to the no flux condition at the outer boundary of the washcoat-wall interface, whereas Eqs. 1 and 2 are subjected to continuity of concentration and flux at the fluid-washcoat interface:

$$n_{\Omega_2} \cdot \nabla_T C_2 = 0 \quad \text{on } \partial\Omega_2 \quad (3a)$$

$$C_1 = C_2 \quad \text{and} \quad n_{\Omega_1} \cdot (D_f \nabla_T C_1 - D_s \nabla_T C_2) = 0 \quad \text{on } \partial\Omega_1 \quad (3b)$$

The inlet and initial conditions are given by

$$C_1 = C^{\text{in}}(x, y, t) \in \Omega_1 \quad \text{at } z = 0 \quad (\text{Inlet}) \quad (3c)$$

$$C_1(x, y, z, t = 0) = C_{10}(x, y, z); C_2(x, y, z, t = 0) = C_{20}(x, y, z) \quad (\text{Initial}) \quad (3d)$$

where C^{in} is the inlet reactant concentration. Here, $\partial\Omega_1$ is the fluid-washcoat interfacial perimeter, $\partial\Omega_2$ is the washcoat-wall boundary, n_{Ω_1} , and n_{Ω_2} are unit outward normals to $\partial\Omega_1$ and $\partial\Omega_2$, respectively, as shown in Figure 1.

We define two characteristic length scales for transverse diffusion associated with the fluid phase (R_{Ω_1}) and the wash-

coat (R_{Ω_2}), respectively. The characteristic length scale for the fluid phase (R_{Ω_1}) is defined as the ratio of the flow area ($A_{\Omega_1} = \int_{\Omega_1} d\Omega$) to the interfacial perimeter (P_{Ω}), whereas the characteristic length or the effective thickness for the washcoat (R_{Ω_2}) is defined as the ratio of washcoat cross-sectional area ($A_{\Omega_2} = \int_{\Omega_2} d\Omega$) to the interfacial perimeter (P_{Ω}). The transverse diffusion length for the fluid phase (R_{Ω_1}) is related to the hydraulic diameter of the channel by $d_h = 4R_{\Omega_1}$.

One-Dimensional Two-Phase Model

Since the solution of detailed model consisting of partial differential equations in time and three spatial coordinates is time consuming (especially for practical cases involving multiple species, nonisothermal effects, time varying inlet conditions, and when the ratio of species diffusivities in the gas phase to that in washcoat is large), simplified models have been proposed for simulating catalytic monoliths. As stated in the introduction, the most widely accepted of these is the two-phase model that uses two representative concentrations at each axial position. For the case of negligible axial dispersion within the fluid phase, this model in dimensional form is given by

$$\frac{\partial C_{\text{fm}}}{\partial t} + \langle u \rangle \frac{\partial C_{\text{fm}}}{\partial z} = -k_{\text{me}} a_v (C_{\text{fm}} - C_s) \quad (4a)$$

$$k_{\text{me}} (C_{\text{fm}} - C_s) = R_s(C_s), \quad (4b)$$

where C_{fm} is cup-mixing concentration in the fluid phase, C_s is concentration at the fluid-washcoat interface, k_{me} is mass transfer coefficient between the fluid and washcoat, a_v is the fluid-washcoat interfacial area per unit volume, and R_s is the reaction rate (calculated per unit interfacial area). In the literature, this model is usually modified to include the diffusional limitations in the solid phase by introducing the effectiveness factor. In this case, Eq. 4b is modified as

$$k_{\text{me}} (C_{\text{fm}} - C_s) = R_{\Omega_2} \eta R(C_s), \quad (4c)$$

where R is volumetric reaction rate (calculated per unit catalyst phase volume) and η is the effectiveness factor defined by

$$\eta = \frac{1}{V_s} \frac{\int R(C) dV_s}{R(C_s)} \quad V_s = \text{volume of washcoat.} \quad (5)$$

This model, which accounts for the local transverse gradients through the concepts of mass transfer coefficient and effectiveness factor, is used extensively in the literature. The problem of flow and diffusion in the gas phase is often decoupled from the reaction in the washcoat and approximated by using a mass transfer coefficient between the bulk fluid phase and the surface. The concept of effectiveness factor is used to simplify the problem of diffusion and reaction in the washcoat. As stated in the introduction, the use of effectiveness factor concept has limitations for the case of multiple reactions. For example, to calculate the volume averaged reaction rates, we need to solve the diffusion-reaction problem in the washcoat, which is numerically intensive, especially for the case of multiple reactions.

A Low-Dimensional Model for an Isothermal Monolith with Washcoat Diffusion

In this section, we present a low-dimensional model that is a generalization of the classical two-phase model. It is derived by averaging the detailed Eqs. 1–3. We define averaged concentrations in fluid phase and washcoat that will be used later in deriving the low-dimensional model. The fluid phase cup-mixing concentration (C_{fm}) is defined as the transverse averaged concentration weighted with respect to the velocity profile, and is given by

$$C_{\text{fm}} = \frac{\int_{\Omega_1} f(x, y) C_1(x, y) d\Omega}{\int_{\Omega_1} f(x, y) d\Omega} = \frac{1}{A_{\Omega_1}} \int_{\Omega_1} f(x, y) C_1(x, y) d\Omega \quad (6a)$$

where $f(x, y)$ is the normalized velocity profile satisfying the relation, $\int_{\Omega_1} f(x, y) d\Omega = A_{\Omega_1}$.

Similarly, the surface concentration C_s , or more precisely, the circumferentially averaged concentration at the fluid-washcoat interface is defined by

$$C_s = \frac{\int_{\delta\Omega_1} C_1(x, y) d\Gamma}{\int_{\delta\Omega_1} d\Gamma} = \frac{\int_{\delta\Omega_1} C_2(x, y) d\Gamma}{\int_{\delta\Omega_1} d\Gamma}, \quad (6b)$$

where $d\Gamma$ is the arc length along the fluid-washcoat interface.

The spatially (or local volume) averaged concentration in the gas phase is defined by

$$\langle C_f \rangle = \frac{\int_{\Omega_1} C_1(x, y) d\Omega}{\int_{\Omega_1} d\Omega} = \frac{1}{A_{\Omega_1}} \int_{\Omega_1} C_1(x, y) d\Omega \quad (6c)$$

The spatially (or local volume) averaged concentration in the washcoat is defined by

$$\langle C_{\text{wc}} \rangle = \frac{\int_{\Omega_2} C_2(x, y) d\Omega}{\int_{\Omega_2} d\Omega} = \frac{1}{A_{\Omega_2}} \int_{\Omega_2} C_2(x, y) d\Omega \quad (6d)$$

We also define the average external mass transfer coefficient between the bulk of fluid phase and fluid-washcoat interface by

$$k_{\text{me}} = \frac{Sh_e D_f}{4R_{\Omega_1}} = -\frac{1}{P_{\Omega}} \frac{\int_{\delta\Omega_1} D_f (\nabla_T C_1) \cdot n_{\Omega_1} d\Gamma}{(C_{\text{fm}} - C_s)}, \quad (7a)$$

Similarly, the average internal mass transfer coefficient between the interior of the washcoat and fluid-washcoat interface is defined by

$$k_{\text{mi}} = \frac{Sh_i D_s}{R_{\Omega_2}} = \frac{1}{P_{\Omega}} \frac{\int_{\delta\Omega_1} D_s (\nabla_T C_2) \cdot n_{\Omega_1} d\Gamma}{(C_s - \langle C_{\text{wc}} \rangle)} \quad (7b)$$

Integrating Eq. 1 over the cross section of the fluid phase, applying the divergence theorem, the definition of external mass transfer coefficient (Eq. 7a) and the definitions of the averaged concentrations (Eqs. 6a–6c), we get

$$A_{\Omega_1} \frac{\partial \langle C_f \rangle}{\partial t} + \langle u \rangle A_{\Omega_1} \frac{\partial C_{\text{fm}}}{\partial z} = -P_{\Omega} k_{\text{me}} (C_{\text{fm}} - C_s)$$

Neglecting the microscale mixing in the fluid phase or using the approximation ($C_{\text{fm}} \approx \langle C_f \rangle$) and dividing by A_{Ω_1} , we get

$$\frac{\partial C_{\text{fm}}}{\partial t} + \langle u \rangle \frac{\partial C_{\text{fm}}}{\partial z} = -\frac{1}{R_{\Omega_1}} k_{\text{me}} (C_{\text{fm}} - C_s). \quad (8a)$$

Integrating Eq. 2 over the cross section of washcoat, applying the divergence theorem, the definitions of internal mass transfer coefficient (Eq. 7b) and the averaged concentrations (Eqs. 6b and 6d), we get

$$\varepsilon_{\text{wc}} A_{\Omega_2} \frac{\partial \langle C_{\text{wc}} \rangle}{\partial t} = k_{\text{mi}} P_{\Omega} (C_s - \langle C_{\text{wc}} \rangle) - \int_{\Omega_2} R(C_2) d\Omega$$

We express the reactant concentration in the washcoat as a sum of the volume averaged concentration and a deviation, that is, $C_2 = \langle C_{\text{wc}} \rangle + C'_2$, so that we have (by definition)

$$\int_{\Omega_2} C'_2 d\Omega = 0.$$

Now, the reaction rate over the volume of the washcoat may be expressed as

$$\begin{aligned} \int_{\Omega_2} R(C_2) d\Omega &= A_{\Omega_2} R(\langle C_{\text{wc}} \rangle) + \frac{\partial R}{\partial C_2} (\langle C_{\text{wc}} \rangle) \int_{\Omega_2} C'_2 d\Omega \\ &+ \frac{1}{2!} \frac{\partial^2 R}{\partial C_2^2} (\langle C_{\text{wc}} \rangle) \int_{\Omega_2} (C'_2)^2 d\Omega + \dots \end{aligned}$$

The second term on the r.h.s. of above equation vanishes and ignoring higher order terms, (assuming $C'_2 \ll \langle C_{\text{wc}} \rangle$), we get the following equation for the averaged form of the species balance in the washcoat:

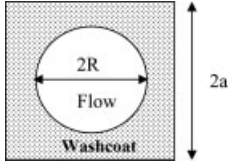
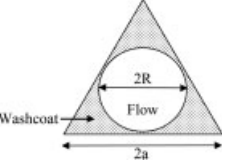
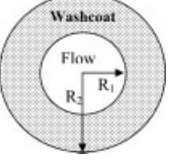
$$\varepsilon_{\text{wc}} R_{\Omega_2} \frac{\partial \langle C_{\text{wc}} \rangle}{\partial t} = k_{\text{mi}} (C_s - \langle C_{\text{wc}} \rangle) - R_{\Omega_2} R(\langle C_{\text{wc}} \rangle) \quad (8b)$$

Integrating Eq. 3b along the circumference at the fluid-washcoat interface and using the definitions of mass transfer coefficients (Eqs. 7a and 7b), we can write,

$$k_{\text{me}} (C_{\text{fm}} - C_s) = k_{\text{mi}} (C_s - \langle C_{\text{wc}} \rangle) \quad (8c)$$

Thus, the problem of diffusion and reaction in the washcoat is accounted for by the use of internal mass transfer coefficient (k_{mi}) and internal concentration gradient, ($C_s - \langle C_{\text{wc}} \rangle$). Similarly, the problem of flow and transverse diffusion in the gas phase is accounted for by the use of the external mass transfer coefficient (k_{me}) and the external concentration gradient, ($C_{\text{fm}} - C_s$). We note that the fluid-washcoat interfacial concentration, C_s , can be eliminated from Eqs. 8a and 8b using (8c) and the low-dimensional model reduces to two-mode form given by

Table 1. Asymptotic Values of External (Sh_e) and Internal (Sh_i) Sherwood Numbers for Some Common Channel and Washcoat Shapes

	$Sh_{e\infty}$	a/R	$Sh_{i\infty}$
	48/11	1	0.826
		1.1	1.836
		1.2	2.533
		1.5	3.716
	$Sh_{e\infty}$		
	48/11	1.7321	0.84
		1.9245	1.45
		2.4744	2.92
		R_2/R_1	$Sh_{i\infty}$
	$Sh_{e\infty}$		
	48/11	1.01	3.015
		1.1	3.153
		1.2	3.311
		1.5	3.818

$$\frac{\partial C_{fm}}{\partial t} + \langle u \rangle \frac{\partial C_{fm}}{\partial z} = -\frac{1}{R_{\Omega_1}} k_{mo} (C_{fm} - \langle C_{wc} \rangle) \quad (9a)$$

$$\varepsilon_{wc} R_{\Omega_2} \frac{\partial \langle C_{wc} \rangle}{\partial t} = k_{mo} (C_{fm} - \langle C_{wc} \rangle) - R_{\Omega_2} R (\langle C_{wc} \rangle) \quad (9b)$$

with the averaged initial and boundary conditions given by

$$C_{fm}(z, t = 0) = C_{fm0}(z) \quad (10a)$$

$$\langle C_{wc} \rangle(z, t = 0) = \langle C_{wc} \rangle_0(z) \quad (10b)$$

$$C_{fm} = C_{in}(t) \text{ at } z = 0. \quad (10c)$$

Here, k_{mo} can be considered as overall mass transfer coefficient, reciprocal of which is the sum of the two resistances of mass transfer, that is, $\frac{1}{k_{mo}} = \frac{1}{k_{me}} + \frac{1}{k_{mi}}$. Table 1 shows asymptotic values (for the case of very slow reaction) of the dimensionless mass transfer coefficients or Sherwood numbers, Sh_e and Sh_i [defined by Eqs. 7a and 7b] for different washcoat and channel geometric shapes. For a detailed discussion on the internal mass transfer coefficient, we refer to another recent publication.²⁴

Equations 9a and 9b represent the low-dimensional two-mode (namely C_{fm} and $\langle C_{wc} \rangle$) model for a laminar flow catalytic monolith with arbitrary channel geometry but with high axial Peclet number (convection dominated limit). We refer to Eq. 8a as the global evolution equation as it describes the evolution of the mixing-cup concentration, C_{fm} with residence time or length along the channel. Equations 8b and 8c are called the local equations because they give the local mass transfer between different scales due to the coupling between reaction and flow and are dependent only on local variables like local diffusion lengths, local reaction rate and the species diffusivities (D_f , D_s).

Physics of the catalytic monolith explained by low-dimensional model

In this sub-section, we explain the physics of the catalytic monolith (gas–solid mass transfer with chemical reaction) using the above low-dimensional model. We also explain the physical significance of multiple concentrations or “modes” used in the low-dimensional model.

In conventional mass/heat transfer, we use the concept of transfer coefficients based on the assumption that the resistance to diffusion of mass/heat can be described by a fictitious stagnant film of certain thickness within which the concentration or temperature variation occurs. When there are multiple resistances in series, the mass/heat flux is proportional to an overall driving force or gradient for transfer. In this case, resistances to transfer in multiple phases are added to get an overall resistance. The reciprocal of the overall resistance is an overall coefficient, which is more convenient to use for design calculations than the individual coefficients.

We can extend this concept to explain the physics of gas–solid mass transfer with chemical reaction in the washcoated monolith. The simplified low-dimensional model considers mass transfer as a combined effect of inter- and intraphase gradients and is an extension of the classical two-phase model. We write two separate equations for the fluid and solid phases. Figure 2 shows local gas–solid mass transfer with chemical reaction at an intermediate section of the catalytic monolith. Reactants in the gas phase diffuse from the bulk to the gas–solid interface and they simultaneously diffuse and react within the solid phase. This may be explained by a hypothetical two-resistance model. The resistance for mass transfer in the gas phase resides in the stagnant film of certain thickness in which concentration drops from C_{fm} to C_s (at gas–solid interface). Similarly, in the solid phase, the resistance to mass transfer is located near a thin region (or boundary layer) near the gas–solid interface and the concentration drops from C_s (at gas–solid interface) to $\langle C_{wc} \rangle$ in the bulk solid (washcoat) phase. In the bulk solid (catalyst) phase, we assume that the concentration is constant at $\langle C_{wc} \rangle$. The reaction rate is evaluated at this volume averaged concentration. From the physics of the gas–solid mass transfer with chemical reaction, it is clear that we need three modes

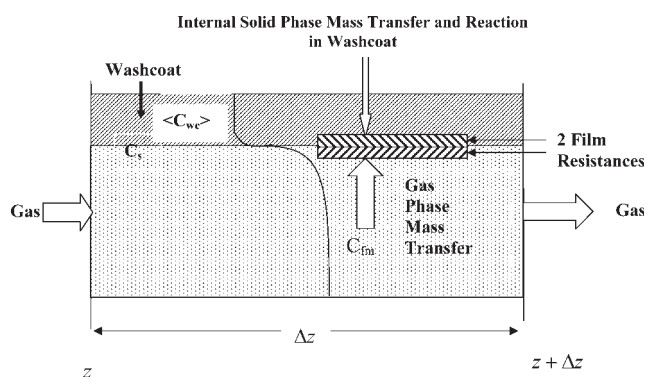


Figure 2. Local gas–solid mass transfer with chemical reaction in the washcoat with two film resistances.

or concentrations (namely, C_{fm} , C_s , $\langle C_{wc} \rangle$) to model the local gradients in the system.

Comparison of low-dimensional model with conventional two-phase model

In this sub-section, we show how the low-dimensional model reduces to the conventional two-phase model in the limit of vanishingly thin washcoat. For a very thin washcoat, $R_{\Omega_2} \rightarrow 0$, and $C_s = \langle C_{wc} \rangle$. The reaction rate per unit fluid-washcoat interfacial area can be calculated from volumetric reaction rate as

$$R_s(C_s) = \frac{R_{\Omega_2} R(\langle C_{wc} \rangle) (P_{\Omega} \Delta z)}{(P_{\Omega} \Delta z)} = R_{\Omega_2} R(\langle C_{wc} \rangle). \quad (11)$$

Using Eqs. 8b, 8c, and 11, Eq. 8b reduces to,

$$k_{me}(C_{fm} - C_s) = R_s(C_s) \quad (8b')$$

Thus, by comparing Eqs. 8a and 8b' to 4a and 4b, respectively, it is concluded that the low-dimensional model reduces to conventional two-phase model in the limit of vanishingly thin washcoat. For finite washcoat thickness, the low-dimensional model extends the classical two-phase model by including accumulation terms and concentration gradients in the solid phase but without using the effectiveness factor concept.

Extensions to the low-dimensional model when boundary layers exist

In this sub-section, we present some extensions that expand the range of validity of the low-dimensional model. First, as noted above, the low-dimensional model was derived by assuming that the aspect ratio of the channel is small, that is, the channel length is much larger than the hydraulic diameter. Therefore, we can justify using a constant Sherwood number in describing the external mass transfer. However, if the flow enters the channel fully developed but the residence time is comparable to the transverse diffusion time, we cannot neglect the boundary layer near the entrance. Therefore, the low-dimensional model that is presented above should be used with a position dependent mass transfer coefficient. We can expand the range of validity of our low-dimensional model by making Sh_e position dependent. For example, for a circular channel, position dependent Sh_e is given by,¹³

$$Sh_e(z') = \begin{cases} 2.31(pPe)^{1/3}, & 0 < z' < \frac{0.71}{Pe} \\ 2.065\left(\frac{p}{z'}\right)^{1/3}, & \frac{0.71}{Pe} < z' < 0.1p \\ \frac{48}{11}, & z' > 0.1p \end{cases} \quad (12)$$

where, z' is dimensionless axial distance, p is transverse Peclet number and Pe is axial Peclet number.

Similarly, when the diffusion time within the washcoat is small compared to the characteristic reaction time or when the drop in the concentration within the washcoat is small, ($C'_2 \ll \langle C_{wc} \rangle$), we can justify using a constant internal Sherwood number (Sh_i).²⁴ This assumption may not be valid for fast reactions ($\phi_s \gg 1$) or when the ratio of species diffusiv-

ities in the gas phase to those in the washcoat is large ($D_f/D_s > 100$). For large value of the normalized Thiele modulus (ϕ_s), which for a single step irreversible reaction is defined by

$$\phi_s^2 = \frac{R_{\Omega_2}^2 R(C_s)^2}{2D_s \int_0^{C_s} R(C) dC},$$

the concentration in the solid phase drops very rapidly and a boundary layer exists close to the washcoat-fluid interface. In such cases, we can expand the range of validity of the low-dimensional model for large values of Thiele modulus (ϕ_s) by making Sh_i as a function of ϕ_s . For example, for the general case of a single reaction, Sh_i can be approximated by,²⁴

$$Sh_i = Sh_{i\infty} + \frac{\Lambda \phi_s^2}{1 + \Lambda \phi_s^2}, \quad (13)$$

where the asymptotic Sherwood number ($Sh_{i\infty}$) and the constant Λ depend only on the washcoat geometry (For further discussion about internal Sherwood numbers for the case of single and multiple reactions, we refer to the recent work of Balakotaiah²⁴). Thus, with these modifications, by making Sh_e and Sh_i numbers position dependent, we can expand the region of validity of the low-dimensional model to include most cases of practical interest. Moreover, the dimensionless numbers Sh_e , Sh_i can be calculated or estimated once the flow conditions, reaction system/kinetics and washcoat geometries are known. Once again, the asymptotic values (for the case of very slow reaction) of Sh_e and Sh_i for different washcoat and channel geometric shapes are listed in Table 1.

Accuracy of low-dimensional model for linear kinetics

In this sub-section, we demonstrate the accuracy of the two-mode model by comparing its solution with that of the full partial differential equation (PDE) model. The solution of the latter is obtained by the finite Fourier transformation with the following assumptions: (i) convection is dominant over axial diffusion (axial Peclet number is very large), (ii) isothermal case with first order reaction (Rate = $k C$), (iii) steady state, (iv) fully developed flow in a channel of circular cross-section, and (v) washcoat thickness is small when compared with the channel hydraulic diameter so that curvature effects may be neglected. The resulting model and solution procedure and expressions for the exit cup-mixing concentration in the fluid phase may be found in Bhattacharya et al.²⁵

We compare the predictions of the low-dimensional model with that of the full PDE model in Figure 3 for a typical set of parameter values: $p = \frac{R_{\Omega_1} \langle u \rangle}{D_f L} = 0.025$, $\mu = \frac{D_f}{D_s} = 100$, $\lambda = \frac{R_{\Omega_2}}{R_{\Omega_1}} = 0.2$, $\phi_s = R_{\Omega_2} \sqrt{\frac{k}{D_s}} = 20$. It can be observed that the extended low-dimensional model (with modified Sh_e and Sh_i numbers) using Eqs. 12 and 13 is as accurate as the analytical solution for all practical purposes.

Extension to the Nonisothermal Case

We now present the extension of the low dimensional model for transient simulations under nonisothermal

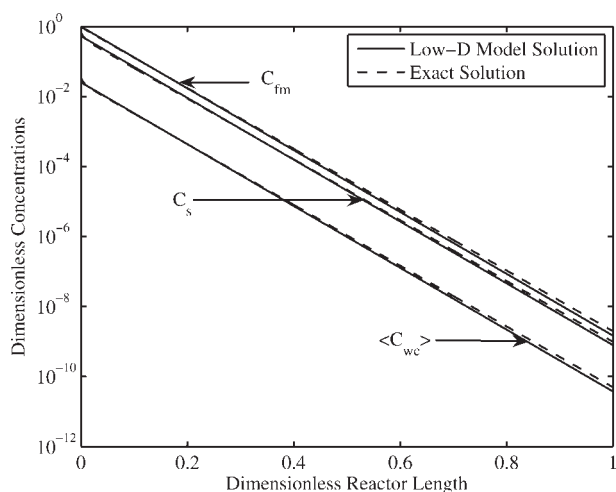


Figure 3. Comparison of low-dimensional model and analytical solutions for an isothermal monolith with linear kinetics.

conditions. While deriving the low-dimensional model, we considered only the species balance. Since we have assumed isothermal conditions, we neglected the energy balance. We can extend the low-dimensional model for the nonisothermal case by adding energy balance equations with coupling between the species and energy balances coming through the reaction terms. Assuming a high thermal diffusivity of solid phase (washcoat and support), we can ignore temperature gradients in the transverse direction in the solid phase. We can write,

$$\frac{\partial C_{fm}}{\partial t} + \langle u \rangle \frac{\partial C_{fm}}{\partial z} = -\frac{1}{R_{\Omega_1}} k_{mo} (C_{fm} - \langle C_{wc} \rangle) \quad (14a)$$

$$\varepsilon_{wc} R_{\Omega_2} \frac{\partial \langle C_{wc} \rangle}{\partial t} = k_{mo} (C_{fm} - \langle C_{wc} \rangle) - R_{\Omega_2} R(\langle C_{wc} \rangle, T_s) \quad (14b)$$

with initial and boundary conditions

$$\begin{aligned} C_{fm}(z, t=0) &= C_{fm0}(z) \\ \langle C_{wc} \rangle(z, t=0) &= \langle C_{wc} \rangle_0(z) \\ C_{fm} &= C_{in}(t) \text{ at } z=0 \end{aligned} \quad (15)$$

The energy balance can be written as,
Fluid phase:

$$\rho_f c_{pf} \frac{\partial T_f}{\partial t} + \langle u \rangle \rho_f c_{pf} \frac{\partial T_f}{\partial z} = -\frac{1}{R_{\Omega_1}} h(z) (T_f - T_s) \quad (16a)$$

Solid phase:

$$\begin{aligned} R_{\Omega_w} \rho_w c_{pw} \frac{\partial T_s}{\partial t} &= R_{\Omega_w} k_w \frac{\partial^2 T_s}{\partial z^2} + h(z) (T_f - T_s) \\ &+ R_{\Omega_2} R(\langle C_{wc} \rangle, T_s) (-\Delta H) \end{aligned} \quad (16b)$$

with initial and boundary conditions

$$\begin{aligned} T_f &= T_{fin}(t) \text{ at } z=0, T_f(z, t=0) = T_{f0}(z), T_s(z, t=0) \\ &= T_{s0}(z), \frac{\partial T_s}{\partial z} = 0 \text{ at } z=0, L \end{aligned} \quad (17)$$

Equations 14a and 14b along with 16a and 16b describe the four-mode (namely C_{fm} , $\langle C_{wc} \rangle$, T_s , T_f) low-dimensional model for the laminar flow nonisothermal catalytic monolith with high thermal diffusivity of solid phase (neglecting transverse temperature gradients in the solid phase). Equations 15 and 17 describe boundary and initial conditions. Here, R_{Ω_2} , R_{Ω_w} are the effective washcoat and wall thickness, respectively. In deriving Eq. 16b, we have assumed that the coefficients of the accumulation and conduction terms in the solid-phase energy balance can be expressed as: $R_{\Omega_w} \rho_w c_{pw} = R_{\Omega_2} \rho_c c_{pc} + R_{\Omega_w} \rho_s c_{ps}$, $R_{\Omega_w} k_w = R_{\Omega_2} k_c + R_{\Omega_w} k_s$, where the subscript s and c refer to the support and washcoat, respectively. Now, we demonstrate the application of four mode low-dimensional model given by Eqs. 14a–17 for simulating the transient behavior of a catalytic monolith for the case of CO oxidation. Further, we validate the four mode model by comparing the solution with the detailed solution obtained by COMSOL [version 3.3, Copyright 1994–2007 by COMSOL]. The oxidation kinetics are taken from the work of Pontikakis and Stamatelos.²⁶

$$\begin{aligned} R &= \frac{1 \times 10^{19} \exp(-10,825/T_s) x_{CO} x_{O_2}}{F(x_{CO}, T_s)}, \\ F(x_{CO}, T_s) &= T_s \left(1 + 65.5 \exp\left(\frac{961}{T_s}\right) x_{CO} \right)^2 \end{aligned} \quad (18a)$$

Here, x_{CO} , x_{O_2} are mole fractions of CO and O_2 in the washcoat, respectively, and T_s is the temperature of the washcoat. Discretizing the equations in the axial direction using the finite difference method results in a set of ODEs which are then integrated in time using semi-implicit integrator to get temperature and concentration profiles at different times. Here, we present the results for the case of a cylindrical monolith with a set of parameter values listed in Table 2. The position dependent heat and mass transfer coefficients are calculated using a correlation¹³:

Table 2. Standard Set of Parameter Values Used for Simulation

$\langle u \rangle$	1 m/s	ρ_f	0.6 kg/m ³
L	7 cm	c_{pf}	1000 J/kg/K
R_{Ω_1}	0.3 mm	ρ_w	2500 kg/m ³
R_{Ω_w}	100 μ m	c_{pw}	1000 J/kg/K
R_{Ω_2}	15 μ m	k_f	0.05 W/m/K
T_{s0}	300 K	k_w	2 W/m/K
Case 1 CO oxidation simulations		Case 2 TWC simulations	
T_{fin}	600 K	T_{fin}	540 K
$x_{CO_{in}}$	1%	$x_{CO_{in}}$	1%
$x_{O_{2in}}$	5%	$x_{HC_{in}}$	500 ppm
		$x_{H_{2in}}$	0.3%
		$x_{O_{2in}}$	0.85%
		$x_{NO_{in}}$	300 ppm

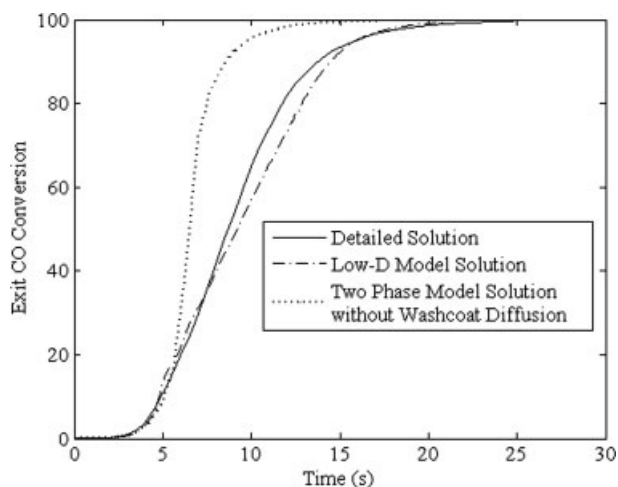


Figure 4. Simulated exit CO conversion in a monolith.

$$Nu(z') = Sh_e(z') = \begin{cases} 2.31(pPe)^{1/3}, & 0 < z' < \frac{0.71}{Pe} \\ 2.065\left(\frac{p}{z'}\right)^{1/3}, & \frac{0.71}{Pe} < z' < 0.1p \\ \frac{48}{11}, & z' > 0.1p \end{cases} \quad (18b)$$

The internal mass transfer coefficient for a cylindrical washcoated monolith is given by²⁴

$$Sh_i = 3 + \frac{0.2\phi_s^2}{1 + 0.2\phi_s} \quad (18c)$$

Diffusivity of species in the gas phase is calculated assuming it is diluted in nitrogen. The diffusion in the pores of a typical monolith reactor washcoat is dominated by Knudsen diffusion and effective diffusion coefficient can be written as following (Mukadi and Hayes¹⁷):

$$D_s = \frac{\varepsilon}{\tau} 97a \left(\frac{T}{M_m} \right)^{0.5} \quad (18d)$$

Here, ε = porosity = 0.41, τ = tortuosity factor = 8, M_m = mol wt (g/mol), a = pore radius = 10 nm.

Figure 4 shows the comparison of exit CO conversion in a monolith calculated using three different models. The low-dimensional model solution has a good agreement with the detailed solution. The two-phase model solution without washcoat diffusion predicts early ignition because of higher rates of internal mass transfer. Therefore, it predicts higher conversions or lower cumulative emissions. Comparison of monolith temperature profiles simulated using low-dimensional model and two phase model without washcoat diffusion is shown in Figure 5. Including diffusional limitations in the washcoat not only delays the ignition but it also shifts the location of ignition further downstream in the monolith. Therefore, the temperature predicted by low-dimensional model is always less than that predicted by two phase model until steady state is reached. This effect becomes more prominent for higher values of feed temperatures.

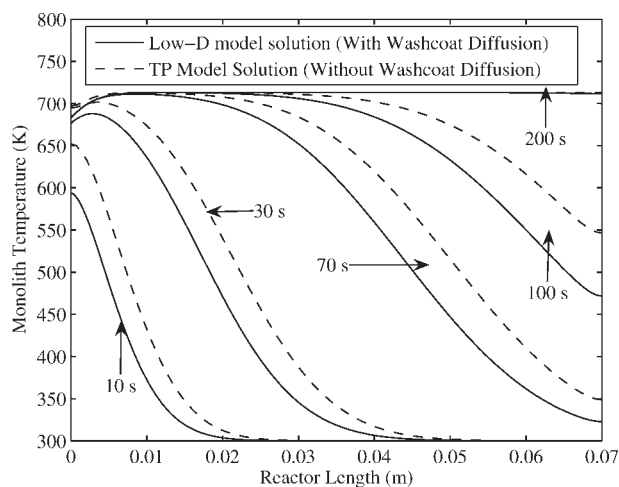


Figure 5. Comparison of simulated monolith temperature profiles for CO Oxidation in a monolith with and without washcoat diffusion.

We now elaborate the rationale behind using three concentrations or modes in the low-dimensional model. Consider the monolith at time, $t = 30$ s. (The axial monolith temperature profile at time, $t = 30$ s is shown in Figure 5). At this time, we can divide the monolith into two parts: ignited (front) part and cold (back) part. In the ignited part of the monolith temperature is very high, reaction rates are very high and therefore the monolith is in the mass transfer controlled regime. The part of the monolith where ignition has not propagated is still cold, reaction rates are small, and the monolith is in the kinetically controlled regime. As time progresses, the ignition front propagates to the back end of the monolith and entire monolith moves into the mass transfer-controlled regime. Figure 6 shows profiles of the three concentrations (c_{fm} , c_s , $\langle c_{wc} \rangle$) at time, $t = 30$ s. It is important to note that in the front (ignited) part of the monolith, there

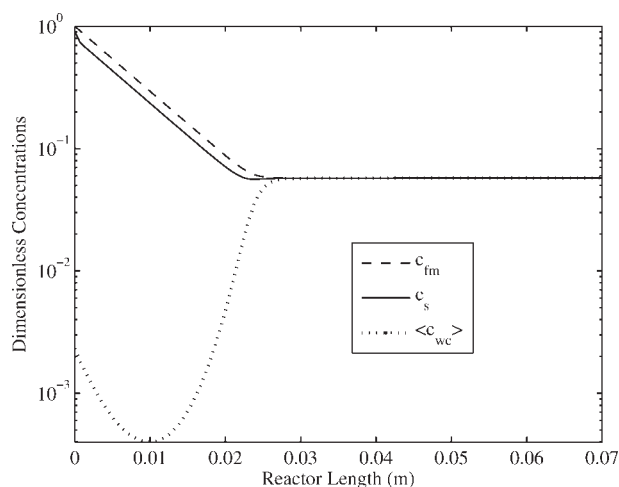


Figure 6. Simulated dimensionless concentration profiles for CO oxidation in a monolith at time, $t = 30$ s, showing strong washcoat diffusional limitations in the ignited part.

is an order of magnitude difference in concentrations c_s , $\langle c_{wc} \rangle$, indicating strong washcoat diffusional limitations. But the back end of the monolith is still cold and there is negligible difference in the concentrations. Thus, by using the difference ($c_s - \langle c_{wc} \rangle$), the low-dimensional model can explain the importance of washcoat diffusion. Similarly, the magnitude of ($c_{fm} - c_s$) indicates the extent of external mass transfer limitations. The overall mass transfer can be described as the combined effect of inter phase gradient ($c_{fm} - c_s$) and internal solid phase gradient ($c_s - \langle c_{wc} \rangle$) which is a measure of diffusional limitations in the washcoat.

Low-Dimensional Model for Multiple Reactions and Nonisothermal Case

In this section, we present an extension of the four mode low-dimensional model to the most general case of multiple reactions under nonisothermal conditions and also show the application of this model for real time simulation of a three-way converter (TWC). The four mode low-dimensional model for the case of multiple reactions can be written as,

$$\frac{\partial C_{fmj}}{\partial t} + \langle u \rangle \frac{\partial C_{fmj}}{\partial z} = -\frac{1}{R_{\Omega_1}} k_{moj} (C_{fmj} - \langle C_{wc} \rangle_j) \quad (19a)$$

$$\begin{aligned} \varepsilon_{wc} R_{\Omega_2} \frac{\partial \langle C_{wc} \rangle_j}{\partial t} &= k_{moj} (C_{fmj} - \langle C_{wc} \rangle_j) \\ &+ R_{\Omega_2} \sum_{i=1}^N v_{ij} R_i (\langle C_{wc} \rangle_1, \langle C_{wc} \rangle_2, \dots, \langle C_{wc} \rangle_s, T_s) \end{aligned} \quad (19b)$$

The initial and boundary conditions are given as,

$$\begin{aligned} C_{fmj}(z, t = 0) &= C_{fmj0}(z) \\ \langle C_{wc} \rangle_j(z, t = 0) &= \langle C_{wc} \rangle_{j0}(z) \\ C_{fmj} &= C_{jin}(t) \text{ at } z = 0 \end{aligned} \quad (20)$$

Here, $j = 1, 2 \dots S$ is the number of species and $i = 1, 2 \dots, N$ is the number of reactions. k_{moj} is the overall mass transfer coefficient for species j , the reciprocal of which is the sum of the two resistances of mass transfer given by $\frac{1}{k_{moj}} = \frac{1}{k_{mij}} + \frac{1}{k_{pej}}$. The external mass transfer coefficient (in the gas phase) is calculated using position dependent $Sh_e(z)$, given by

$$k_{mij}(z) = \frac{Sh_e(z) D_{sj}}{4R_{\Omega_1}}$$

The internal mass transfer coefficient (in the solid phase) for species j is approximated by using the asymptotic internal Sherwood number, $Sh_{i\infty}$:

$$k_{mij} = \frac{Sh_{i\infty} D_{sj}}{R_{\Omega_2}}$$

The energy balances can be written as, Fluid phase:

$$\rho_f c_{pf} \frac{\partial T_f}{\partial t} + \langle u \rangle \rho_f c_{pf} \frac{\partial T_f}{\partial z} = -\frac{1}{R_{\Omega_1}} h(z) (T_f - T_s) \quad (21a)$$

Solid phase:

$$\begin{aligned} R_{\Omega_w} \rho_w c_{pw} \frac{\partial T_s}{\partial t} &= R_{\Omega_w} k_w \frac{\partial^2 T_s}{\partial z^2} + h(z) (T_f - T_s) \\ &+ R_{\Omega_2} \sum_{j=1}^N R_j (\langle C_{wc} \rangle_1, \langle C_{wc} \rangle_2, \dots, \langle C_{wc} \rangle_s, T_s) (-\Delta H_j) \end{aligned} \quad (21b)$$

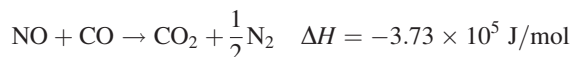
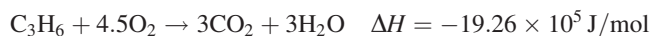
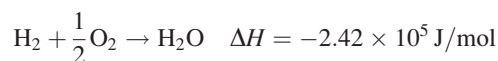
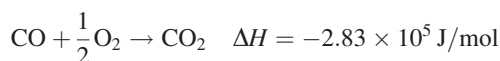
with the following boundary and initial conditions:

$$\begin{aligned} T_f &= T_{fin}(t) \text{ at } z = 0, T_f(z, t = 0) = T_{f0}(z), T_s(z, t = 0) \\ &= T_{s0}(z), \frac{\partial T_s}{\partial z} = 0 \text{ at } z = 0, L \end{aligned} \quad (22)$$

Equations 19a and 19b along with 21a and 21b describe the four-mode (namely C_{fmj} , $\langle C_{wc} \rangle_j$, T_s , T_f) low-dimensional model for laminar flow nonisothermal catalytic monolith with high thermal diffusivity of solid phase (neglecting transverse temperature gradients in the solid phase). The coupling between species and energy balance comes through reaction term in Eqs. 19b and 21b. [Remark: In writing the explicit expressions for the overall mass transfer coefficient for each species, it has been assumed that the species fluxes are decoupled. This assumption leads to a diagonal mass transfer coefficient matrix in the kinetically controlled regime. For further details, we refer to Balakotaiah²⁴].

Application of low-dimensional model for real time simulations of TWC

In this section, we use the low-dimensional model for transient simulations of a three-way converter (TWC). We consider the following reactions:



We use global kinetics, taken from the work of Pontikakis and Stamatelos²⁶

$$R_{\text{CO}} = \frac{k_1 x_{\text{CO}} x_{\text{O}_2}}{G(x, T_s)}, R_{\text{H}_2} = \frac{k_1 x_{\text{H}_2} x_{\text{O}_2}}{G(x, T_s)}$$

where,

$$k_1 = 1 \times 10^{19} \exp(-10,825/T_s), k_3 = 2 \times 10^{19} \exp(-11,427/T_s), (\text{mol K s}^{-1} \text{m}^{-3})$$

$$k_4 = 4 \times 10^{14} \exp(-10,825/T_s), (\text{mol s}^{-1} \text{m}^{-3})$$

$$G(x, T_s) = T_s (1 + k_{a1} x_{\text{CO}} + k_{a2} x_{\text{HC}})^2 (1 + k_{a3} x_{\text{CO}}^2 x_{\text{HC}}^2) (1 + k_{a4} x_{\text{NO}}^{0.7})$$

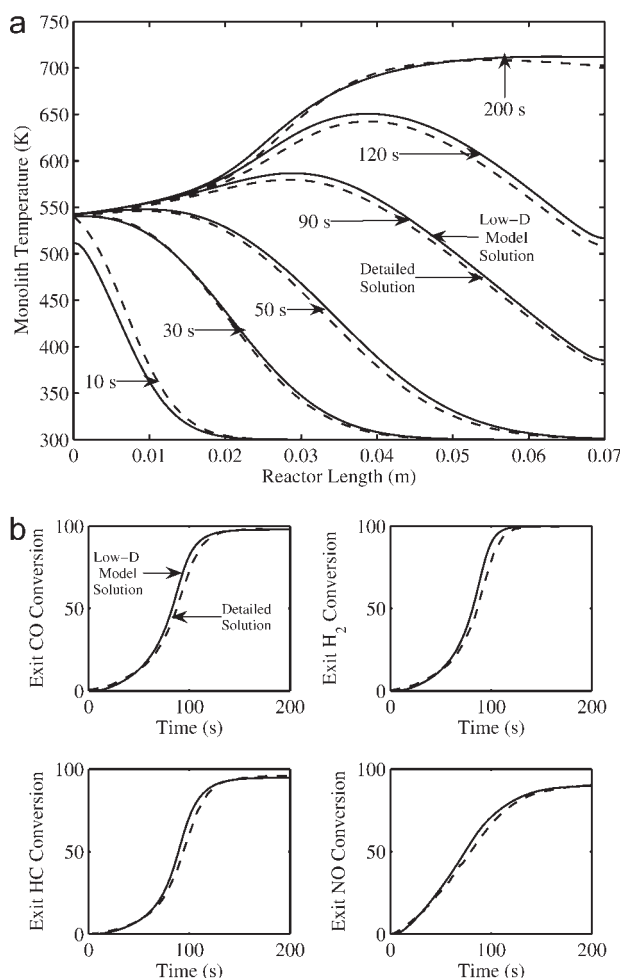


Figure 7. (a) Comparison of monolith temperature at different times predicted by low-dimensional model and detailed solution; (b) comparison of exit conversions predicted by low-dimensional model and detailed solution.

$$k_{a1} = 65.5 \exp(961/T_s), k_{a2} = 2080 \exp(361/T_s),$$

$$k_{a3} = 3.98 \exp(11,611/T_s)$$

$$k_{a4} = 4.79 \times 10^5 \exp(-3733/T_s),$$

x_{CO} , x_{O_2} , x_{HC} , x_{H_2} , x_{NO} are mole fractions of CO, O₂, hydrocarbon, H₂ and NO in the washcoat, respectively. T_s is the temperature of washcoat. Diffusivity of species in the gas phase is calculated assuming it is diluted in nitrogen. The effective diffusion coefficient in the washcoat is calculated using Eq. 18b.

We use four mode low-dimensional model given by Eqs. 19a, 19b and 21a, 21b. Discretizing the equations in the axial direction using finite difference method results in a set of ODEs which are then integrated in time using semi-implicit integrator to get temperature and concentration profiles at different times. In the next section, we compare the low-dimensional model solution with the detailed solution for the case of a cylindrical monolith with standard parameter values listed in Table 2.

Low-dimensional model simulation results and comparison with detailed solution

The detailed solution is obtained by COMSOL [version 3.3, Copyright 1994-2007 by COMSOL]. Figures 7a,b show the comparison of monolith temperature and exit conversions respectively, calculated using COMSOL and the four mode low-dimensional model. Middle ignition is observed and as time progresses it propagates to back end of the monolith. There is a good agreement between the low-dimensional model solution and the detailed solution obtained using COMSOL. The low-dimensional model requires considerably less computation time as compared to COMSOL. To give a comparison to simulate a real time of 200 s, COMSOL takes 2543 s while low-dimensional model can simulate the same problem using MATLAB[®] in 5 s (on a PC with an AMD Athlon 64 Processor 2.41 GHz CPU and 960 MB memory). When the ratio of diffusivities of gas to solid phase is high ($D_f/D_s > 100$) or inlet temperature of fluid is high ($T_{\text{fin}} > 600$ K), the concentration in the washcoat drops very rapidly and a very fine mesh needs to be generated in the washcoat which makes COMSOL simulation extremely slow or in many cases it fails (either due to memory requirement or stiffness caused by the boundary layers appearing). However, the low-dimensional model is robust and can simulate the problem for any parameter value of practical interest within a few seconds. Thus, as stated in the introduction, the main advantage of the low-dimensional model is the speed-up of the calculations by several orders of magnitude while retaining the accuracy. Based on this and other comparisons, we conclude that for all practical purposes, the low dimensional model has practically the same accuracy as the detailed model and can be used with confidence for the design and real time simulation of catalytic monoliths.

Step change in temperature

In the previous section, we presented low-dimensional model simulations for the case of constant inlet temperature and concentrations. But the inlet conditions to the catalytic monolith used in automotive applications are highly transient. Therefore, the application of the low-dimensional model presented above should be justified under such conditions. We demonstrate the application of the low-dimensional model under transient inlet conditions by simulating the transient response of the catalytic monolith after a step increase in the feed temperature. Initially, the monolith is operating under steady state conditions with typical parameter values listed in Table 2. Now the feed temperature is increased to 640 K keeping all other parameters constant. The transient fluid and solid temperature profiles are shown in Figure 8. Initially, there is a middle ignition. As the feed temperature is increased to 640 K, the front portion of the monolith gets heated by convective heat transfer. Because of higher temperatures and higher rates of reaction, ignition shifts to the front part of monolith where most of the reactants get consumed and there is practically no heat generation in middle and back end of the monolith. During initial start up, middle part of the monolith loses heat rapidly by convection and shows a minimum in the temperature. The reaction exotherm generated in the front part is constantly carried downstream by convection

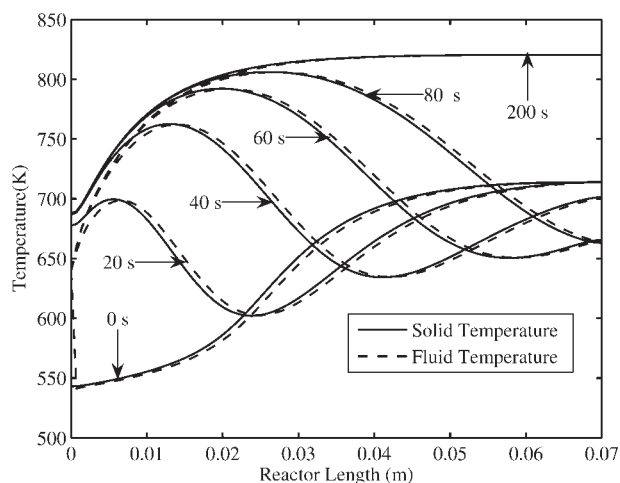


Figure 8. Simulated transient fluid and solid temperature profiles in a TWC for a step increase in feed temperature.

in fluid phase and axial conduction in solid phase and finally, after 200 s, the monolith approaches a new steady state.

Importance of washcoat diffusion

In this section, we study the role of washcoat diffusion in predicting the cold-start behavior of the TWC and cumulative emissions using the low-dimensional model. We compare the low-dimensional model solution with washcoat diffusion and the two-phase model solution without washcoat diffusion. The two-phase model solution is obtained by assuming uniform concentration in the washcoat in transverse direction.

A feed temperature of 650 K is used in the simulations, rest of the parameters are same as those listed in Table 2. Figure 9a shows the transient monolith temperature with and without washcoat diffusion. It should be pointed out that neglecting washcoat diffusion predicts early light-off as it results in higher rates of internal solid phase mass transfer and hence higher rates of reactions. When washcoat diffusion is included, not only the light-off is delayed but also the location gets shifted from the front end to further downstream as shown in Figure 9a. Moreover, the maximum solid temperature is always lower for the case of washcoat diffusion until steady state is reached as shown by Figure 9b. Thus, we observe lower exit conversions with washcoat diffusion as shown in Figure 10. Table 3 shows the percentage error in cumulative emissions for first 100 s when washcoat diffusion is neglected. It is important to note that neglecting washcoat diffusion results in significant error in predicting cumulative emissions for hydrocarbon, CO and NO. Because the diffusivity of hydrogen is high, neglecting washcoat diffusion does not result in significant error in cumulative emissions of H₂.

Conclusions and Discussion

The main contribution of this work is the development of a new low-dimensional model for real time simulations of catalytic reactions in monoliths. The new model is derived directly by averaging the governing equations and using the concepts of internal and external mass transfer coefficients.

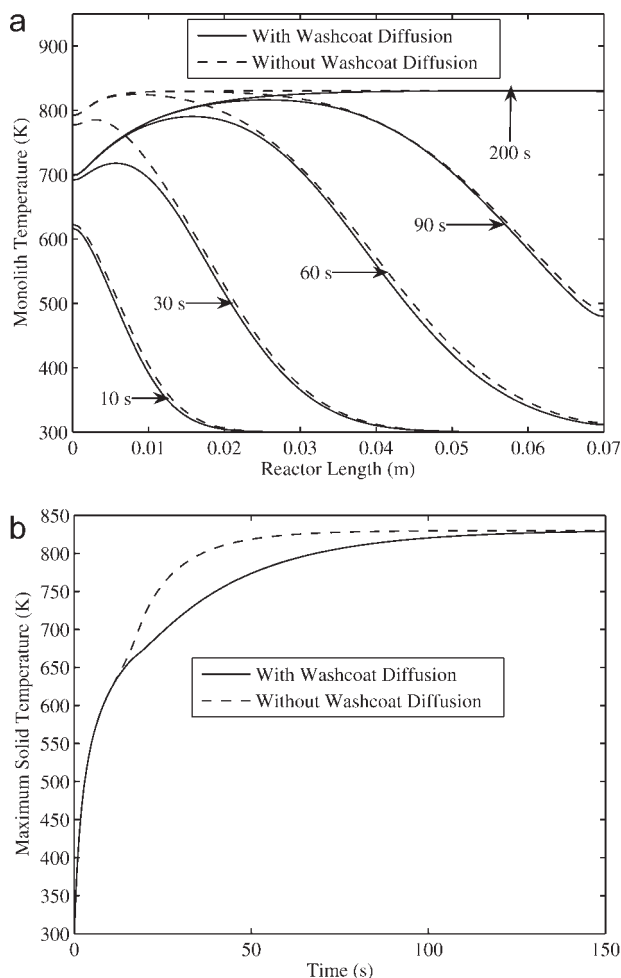


Figure 9. (a) Comparison of monolith temperature in the TWC with and without washcoat diffusion; (b) comparison of maximum solid temperature in the TWC with and without washcoat diffusion.

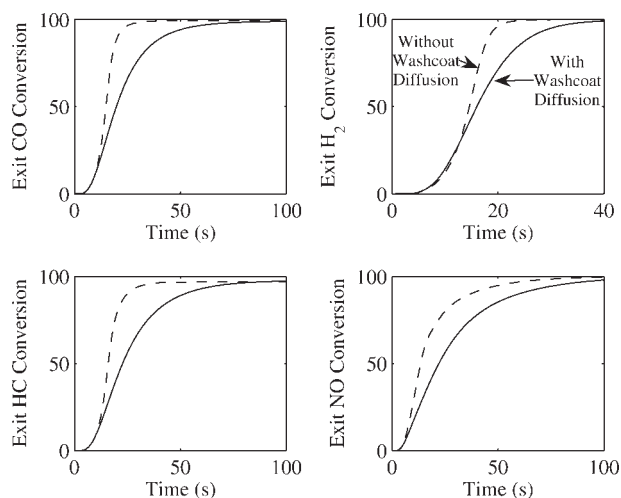


Figure 10. Comparison of exit conversions in the TWC with and without washcoat diffusion.

Table 3. Error in Cumulative Emissions for First 100 s when Washcoat Diffusion is Neglected

Species	% Error in Cumulative Emissions
HC	31.95
CO	34.41
H ₂	16.14
NO	34.89

A major advantage of the new model compared to the more extensively used two-phase models of catalytic reactors is that it includes washcoat diffusional effects without explicitly solving the multicomponent diffusion-reaction problem in the washcoat. The new multimode model captures all the important features involving exchange of mass and thermal energy between different phases. It describes mass transfer as the combined effect of external or interphase gradient ($C_{fm} - C_s$) and intraphase gradient ($C_s - \langle C_{wc} \rangle$) in the washcoat. The low dimensional model reduces the number of equations to be solved retaining all the parameters and essential physics of the full convection-diffusion-reaction model. It speeds up the transient as well as steady-state calculations by orders of magnitude while retaining the accuracy needed for most practical applications.

The low-dimensional model presented here can be extended to include more detailed or microkinetic models, oxygen or NO_x storage, axial activity variations, and time varying inlet conditions or periodic operation. These and other extensions will be considered in future work.

Acknowledgments

This work was supported by a grant from the Ford Motor Company. Partial support was also provided by U.S. DOE National Energy Technology Laboratory (DE-FC26-05NT42630).

Notation

a_v = fluid-washcoat interfacial area per unit volume, m²/m³
 C_1 (C_2) = reactant concentration in fluid phase (washcoat), mol/m³
 C_{fm} = cup-mixing concentration in fluid phase, mol/m³
 C_s = fluid-washcoat interfacial concentration, mol/m³
 $\langle C_{wc} \rangle$ = local volume averaged concentration in the washcoat, mol/m³
 c_{pf} = specific heat of gas, J/kg/K
 c_{pw} = specific heat of solid, J/kg/K
 D_f = molecular diffusivity of the reactant in the fluid phase, m²/s
 D_s = effective diffusivity of the reactant within washcoat, m²/s
 $f(x,y)$ = local fluid phase velocity profile
 h = heat transfer coefficient, J/m²/K/s
 k_{me} = external mass transfer coefficient from the bulk of fluid phase to fluid-washcoat interface, m/s
 k_{mi} = internal mass transfer coefficient between the interior of the washcoat and fluid-washcoat interface, m/s
 k_w = thermal conductivity of the solid, W/m/K
 L = length of the channel, m
 p = transverse Peclet number
 Pe = axial Peclet number
 P_Ω = wetted fluid-washcoat interfacial perimeter, m
 R = reaction rate calculated per unit catalyst phase volume, mol/m³/s
 R_s = reaction rate calculated per unit interfacial area, mol/m²/s
 R_{Ω_1} (R_{Ω_2}) = effective transverse diffusion length for flow (washcoat) area, m
 R_{Ω_w} = effective wall thickness, m
 R_Ω = half thickness of the solid wall without washcoat, m

Sh_e = external Sherwood number
 Sh_i = internal Sherwood number
 T_f = cup-mixing temperature of fluid phase, K
 T_s = solid phase temperature, K
 $\langle u \rangle$ = average fluid velocity, m/s
 x,y = transverse coordinate
 z = axial coordinate

Greek letters

ε_f (ε_s) = volume fraction of fluid phase (washcoat)
 ε_{wc} = porosity of washcoat
 λ = ratio of transverse diffusion lengths of washcoat to fluid phase
 μ = ratio of reactant diffusivities in the fluid phase and the washcoat
 ν = stoichiometric coefficient
 η = effectiveness factor
 ρ_f = density of gas, kg/m³
 ρ_w = density of solid, kg/m³
 ∇_T^2 = transverse Laplacian operator
 $\partial\Omega_1$ ($\partial\Omega_2$) = solid-fluid interfacial (outer channel wall) boundary
 Ω_1 (Ω_2) = cross-sectional domain of fluid phase (washcoat)
 ϕ_s = Thiele modulus

Literature Cited

- Froment GF, Bischoff KB. *Chemical Reactor Analysis and Design*, 2nd ed. New York: Wiley, 1990.
- Oh SH, Cavendish JC. Transients of monolithic catalytic converters: response to step changes in feed stream temperature as related to controlling automobile emissions. *Ind Eng Chem Prod Res Dev*. 1982;21:29–37.
- Hayes RE, Kolaczowski ST, Thomas WJ. Finite Element model for a catalytic monolith reactor. *Comput Chem Eng*. 1992;16:645–657.
- Hawthorn RD. Afterburner catalysts-effects of heat and mass transfer between gas and catalyst surface. *AIChE Symp Ser* 70. 1974; 137:428–438.
- Ullah U, Waldram SP. Monolithic reactors: mass transfer measurements under reacting conditions. *Chem Eng Sci*. 1992;47:2413–2418.
- Uberoi M, Pereira C. External mass transfer coefficients for monolith catalysts. *Ind Eng Chem Res*. 1996;35:113–116.
- Holmgren A, Andersson B. Mass transfer in monolith catalysts-CO oxidation experiments and simulations. *Chem Eng Sci*. 1998;53: 2285–2298.
- West DH, Balakotaiah V, Zoran J. Experimental and theoretical investigation of the mass transfer controlled regime in catalytic monoliths. *Catal Today*. 2003;88:3–16.
- Shah RK, London AL. *Laminar Flow Forced Convection in Ducts, Advances in Heat Transfer (suppl. 1)*. New York: Academic Press, 1978.
- Groppi G, Tronconi E. Theoretical analysis of mass and heat transfer in monolith catalysts with triangular channels. *Chem Eng Sci*. 1997;52:3521–3526.
- Tronconi E, Forzatti P. Adequacy of lumped parameter models for SCR reactors with monolithic structures. *AIChE J*. 1992;38:201–210.
- Halys RE, Kolaczowski ST. Mass and heat transfer effects in catalytic monolith reactors. *Chem Eng Sci*. 1994;49:3587–3599.
- Balakotaiah V, Gupta N. Heat and mass transfer coefficients in catalytic monoliths. *Chem Eng Sci*. 2001;6:4771–4786.
- Balakotaiah V, West DH. Shape normalization and analysis of the mass transfer controlled regime in catalytic monoliths. *Chem Eng Sci*. 2002;57:1269–1286.
- Santos H, Costa M. The relative importance of external and internal transport phenomena in three way catalysts. *Int J Heat Mass Transfer*. 2008;51:1409–1422.
- Santos H, Costa M. Analysis of the mass transfer controlled regime in automotive catalytic converters. *Int J Heat Mass Transfer*. 2008; 51:41–51.

17. Mukadi LS, Hayes RE. Modelling the three-way catalytic converter with mechanistic kinetics using the Newton-Krylov method on a parallel computer. *Comput Chem Eng.* 2002;26:439–455.
18. Koci P, Kubicek M, Marek M. Modeling of three-way-catalyst monolith converters with microkinetics and diffusion in the wash-coat. *Ind Eng Chem Res.* 2004;43:4503–4510.
19. Koltsakis GC, Konstantinidis PA, Stamatelos AM. Development and application range of mathematical models for 3-way catalytic converters. *Appl Catal B: Environ.* 1997;12:161–191.
20. Tischer S, Correa C, Deutschmann O. Transient three-dimensional simulations of a catalytic combustion monolith using detailed models for heterogeneous and homogeneous reactions and transport phenomena. *Catal Today.* 2001;69:57–62.
21. Wanker R, Raupenstrauch H, Staudinger G. A fully distributed model for the simulation of a catalytic combustor. *Chem Eng Sci.* 2000;55:4709–4718.
22. Hayes RE, Kolaczowski ST, Thomas WJ, Titiloye J. Transient experiments and modeling of the catalytic combustion of methane in a monolith reactor. *Ind Eng Chem Res.* 1996;35:406–414.
23. Zygmourakis K. Transient operation of monolith catalytic converters: a two-dimensional reactor model and the effects of radially nonuniform flow distributions. *Chem Eng Sci.* 1989;44:2075–2086.
24. Balakotaiah V. On the relationship between Aris and Sherwood numbers and friction and effectiveness factors. *Chem Eng Sci.* 2008;63:5802–5812.
25. Bhattacharya M, Harold MP, Balakotaiah V. Mass-transfer coefficients in washcoated monoliths. *AIChE J.* 2004;50:2939–2955.
26. Pontikakis G, Stamatelos A. Identification of catalytic converter kinetic model using a genetic algorithm approach. *Proc Inst Mech Eng Part D-J Automob Eng* 2004;218:1455–1472.

Manuscript received Jun. 17, 2008, and revision received Nov. 3, 2008.